

## Effect of noncircular orifice plates on the near flow field of turbulent free jets

This content has been downloaded from IOPscience. Please scroll down to see the full text.

2014 Chinese Phys. B 23 124703

(<http://iopscience.iop.org/1674-1056/23/12/124703>)

View [the table of contents for this issue](#), or go to the [journal homepage](#) for more

Download details:

IP Address: 132.174.250.220

This content was downloaded on 08/07/2017 at 20:01

Please note that [terms and conditions apply](#).

You may also be interested in:

[Mean and fluctuating velocity fields of a diamond turbulent jet](#)

Xu Min-Yi, Zhang Jian-Peng, Mi Jian-Chun et al.

[Investigation of the near-field structure of an elliptic jet using stereoscopic PIV](#)

Jong-Hwan Yoon and Sang-Joon Lee

[Turbulent flow downstream of a large solidity perforated plate: near-field characteristics of interacting jets](#)

Stefan Horender

[Analytical investigation on mean and turbulent velocity fields of a plane jet](#)

Mi Jian-Chun and Feng Bao-Ping

[Experimental investigation on the mean flow field and impact force of a semi-confined round impinging jet](#)

X K Wang, G-P Niu, S-Q Yuan et al.

[An experimental study of a jet with local buoyancy enhancement](#)

R Elavarasan, G S Bhat, R Narasimha et al.

[Image processing analysis of vortex dynamics of lobed jets from three-dimensional diffusers](#)

Ilinca Nastase, Amina Meslem and Mouhammad El Hassan

[On the near-field of a square jet with vortex-generating tabs](#)

X K Wang, L P Chua and S C M Yu

[Influences of initial velocity, diameter and Reynolds number on a circular turbulent air/air jet](#)

Mi Jian-Chun and Du Cheng

# Effect of noncircular orifice plates on the near flow field of turbulent free jets\*

Xu Min-Yi(徐敏义)<sup>a)†</sup>, Tong Xing-Qing(童杏清)<sup>a)</sup>, Yue Dan-Ting(岳丹婷)<sup>a)</sup>,  
Zhang Jian-Peng(张健鹏)<sup>b)</sup>, Mi Jian-Chun(米建春)<sup>b)</sup>, Nathan G. J.<sup>c)</sup>, and Kalt P. A. M.<sup>c)</sup>

<sup>a)</sup>Marine Engineering College, Dalian Maritime University, Dalian 116026, China

<sup>b)</sup>State Key Laboratory of Turbulence & Complex Systems, College of Engineering, Peking University, Beijing 100871, China

<sup>c)</sup>Centre for Energy Technology and School of Mechanical Engineering, University of Adelaide, SA 5005, Australia

(Received 20 March 2014; revised manuscript received 12 June 2014; published online 10 October 2014)

In this paper, we experimentally investigate the near-field flow characteristics of turbulent free jets respectively issued from circular, triangular, diamond, rectangular, and notched-rectangular orifice plates into air surroundings. All the orifice plates have identical opening areas or equivalent diameters ( $D_e$ ) and their aspect ratios ( $AR$ ) range from 1 to 6.5. Planar particle image velocimetry (PIV) is used to measure the velocity field at the same Reynolds number of  $Re = 5 \times 10^4$ , where  $Re = U_e D_e / \nu$  with  $U_e$  being the exit bulk velocity and  $\nu$  the kinematic viscosity of fluid. The mean and turbulent velocity fields of all the five jets are compared in detail. Results show that the noncircular jets can enhance the entrainment rate, reflected by the higher acceleration rates of mean velocity decay and spread, shorten the length of the unmixed core, expedite the increase of turbulent intensity compared with the circular counterpart shortened unmixed core, and increase turbulent intensity comparing to the circular counterpart. Among the five jets, the rectangular jet ( $AR = 6.5$ ) produces the greatest decay rate of the near-field mean velocity, postpones the position at which the ‘axis-switching’ phenomenon occurs. This supports that axis switching phenomenon strongly depends on jet initial conditions. In addition, the hump in the centerline variation of the turbulence intensity is observed in the rectangular and triangular jets, but not in the circular jet, nor in diamond jet nor in notched-rectangular jet.

**Keywords:** noncircular jet, free jet, turbulence mixing, axis-switching

**PACS:** 47.27.wg, 47.80.Cb, 47.85.lk

**DOI:** 10.1088/1674-1056/23/12/124703

## 1. Introduction

Turbulent jets have been widely investigated as they are key devices in many applications such as combustor injection systems, jet propulsions, jet pumps, etc.,<sup>[1–3]</sup> and they have more effective mixing behavior than other systems. Compared with circular jets, noncircular jets have been extensively studied experimentally<sup>[4–11]</sup> and numerically<sup>[12–15]</sup> in the past three decades due to their higher mixing and entrainment rates. Previous studies have shown that the sharp corners and non-uniform curvature of the nozzle can accelerate the formation of three-dimensional turbulent structures in the near field, thus increasing the mixing capability of noncircular jets.<sup>[4]</sup> As the most important feature of noncircular jet, the ‘axis-switching’ phenomenon is the deformation of a vortex ring due to the corner vortices. It strongly affects the turbulent structure and induces a higher entrainment rate in comparison with a circular jet.<sup>[4,14,16,17]</sup> As it occurs in a large scale noncircular jet, the ‘axis-switching’ phenomenon has also been found in a micro-jet despite relatively low Reynolds number.<sup>[18]</sup>

Although the noncircular jets have been extensively investigated previously,<sup>[4,7,8,19–21]</sup> the detailed and direct comparison of the statistical properties among noncircular jets

with different shapes have been rarely reported. As is well known, jet exit conditions, such as nozzle type,<sup>[22,23]</sup> and the exit Reynolds number,<sup>[24–27]</sup> have significant influences on the large-scale and small-scale turbulent statistical properties in the near field flow, even in the far field. In addition, different apparatus and measurement techniques have led to non-negligible differences in various time-averaged data, indicated by Husain and Hussain<sup>[21]</sup> and Dowling and Dimotakis.<sup>[28]</sup> It is therefore difficult to directly compare the results obtained by using different experimental arrangements and different experimental techniques.

Therefore, it is necessary to perform the comparisons among different noncircular jets at the same Reynolds number and the same experimental setup. Hashiehbaaf and Romano<sup>[6]</sup> investigated free jets issuing, respectively, from circular, rectangular, square, triangular, and elliptic sharp edge nozzles by using particle image velocimetry (PIV). They recognized two distinct pairs at low Reynolds number, i.e., square and triangular jets closer to axial-symmetric conditions, and rectangular and elliptic jets with elongated nozzle. The reason for such a difference is that the axis-switching phenomenon in a rectangular or elliptic jet causes a rearrangement of turbu-

\*Project supported by the Fundamental Research Funds for the Central Universities, China (Grant No. 3132014050), the General Science Research Project of the Education Department of Liaoning Province, China (Grant No. L2013198), the Natural Science Foundation of Liaoning Province, China (Grant No. L2014025012), and the National Natural Science Foundation of China (Grant Nos. 10921202 and 11072005).

†Corresponding author. E-mail: xuminyi@dlmu.edu.cn

lence over different velocity components and directions. The velocities and pressure fields in triangular, elliptic, rectangular, square turbulent free jets have been measured by Quinn *et al.*<sup>[5,20,29–33]</sup> The results of the mean streamwise centerline velocity decay, mass entrainment, and jet spreading suggested that the mixing rate in the near field of noncircular jet is higher than that of a corresponding round jet. From the investigation of the noncircular jets, Quinn<sup>[33]</sup> found that the equilateral triangular jet had a higher mixing rate than the isosceles triangular jet and the round jet in the near flow field. Also the mixing rate increases as the aspect angle of isosceles triangular orifice decreases. This is consistent with the studies in elliptic and rectangular jets,<sup>[19–21]</sup> whose large aspect ratio enhances mixing in the near field. Kanamori *et al.*<sup>[34]</sup> experimentally investigated the flow behavior and impinging heat transfer characteristics of turbulent jets issuing, respectively, from regular triangular, square, pentagonal, and hexagonal nozzles. One of the important observations for the flow characteristics is that the location of one complete cycle of axis-switching shifts toward the downstream part of the jet with reducing the number of polygon sides. Mi and Nathan<sup>[9]</sup> and Mi *et al.*<sup>[35]</sup> studied the centerline statistics in turbulent free jets issuing, respectively, from a round nozzle of smooth contraction (SC) and eight (sharp-edged) orifice plates (OP) with different shapes and nearly identical opening areas using hot-wire anemometer. It is demonstrated that the asymmetry of the exit generally causes the mean velocity decay to turn faster and the fluctuating intensity to grow in the near field. In the far field, insignificant differences occur in jet multi-scale turbulent statistics. Among the nine free jets, the isosceles triangular orifice-plate has the most irregular and complex structures which produces the greatest decay rate in the near-field mean velocity. The instantaneous, mean and fluctuating velocity fields in free jets issuing, respectively, from notched-rectangular, triangular, diamond orifice were measured and studied using PIV by Mi *et al.*<sup>[36]</sup> and Xu *et al.*<sup>[7,8]</sup> Consistent with previous studies about noncircular jet, the results show that all the noncircular jets enhance mixing compared with circular counterpart, as the axis-switching phenomenon makes the vortex structures in the near field three-dimensional.

Despite the fact that Mi and Nathan<sup>[9]</sup> and Mi *et al.*<sup>[35]</sup> compared and reported the centerline statistical properties of jet flows issuing, respectively, from nine nozzles with different shapes, measured by using a hot-wire anemometer, the radial turbulent statistic profiles and axis-switching phenomenon were not present. In addition, Mi *et al.*<sup>[27]</sup> indicated that jet flows have two turbulent regimes. One is to develop or partially develop turbulence at  $Re < Re_{cr}$  where  $Re_{cr}$  is the critical Reynolds number, and the other is to fully develop turbulence at  $Re > Re_{cr}$ . The critical Reynolds number varies from flow to flow, such as  $Re_{cr} \approx 1 \times 10^4$  for the circular

jet while  $Re_{cr} \approx 3 \times 10^4$  for the square jet.<sup>[26]</sup> However, Mi and Nathan,<sup>[9]</sup> Mi *et al.*<sup>[35]</sup> chose Reynolds numbers such that approximately an identical value of  $Re$  is  $1.5 \times 10^4$ , i.e.,  $Re = 1.5 \times 10^4$ . Thus, the noncircular jets studied by Mi *et al.*<sup>[9,35]</sup> may be not fully developed.

To compare the statistical velocity fields of noncircular jets and to minimize the experimental uncertainty and the effect of the Reynolds number, we measure (using PIV technique) the velocity fields for jet flows issuing, respectively, from circular, triangular, diamond, rectangular, notched-rectangular orifice plates with nearly identical opening areas. The value of Reynolds number for the five jet flows is  $Re = 5 \times 10^4$ , which is higher than that used in Mi *et al.*'s previous study about noncircular jets.<sup>[9,35]</sup> Despite our previous work, in which based on the same measurements, the jet flows issuing, respectively, from circular and notched-rectangular,<sup>[36]</sup> triangular,<sup>[7]</sup> and diamond<sup>[8]</sup> orifices were compared and reported, it is necessary to make detailed and direct comparison among the above four jets, as well as a rectangular jet.

## 2. Experimental details

Figure 1 shows the supply tube of 25.4 mm in diameter and 1000 mm in length, to which is attached an orifice plate, and the shapes and dimensions of the five orifice plates reported in the present study. These orifices have nominally the same opening area ( $A$ ) and thus a nearly identical equivalent diameter  $D_e [\equiv 2(A\pi^{-1})^{1/2}]$  of approximately 12 mm. Accordingly, the ratio of the plenum pipe diameter to  $D_e$  is about 2.1. For the present study, aspect ratios ( $AR$ ) is defined as the ratio between the two (long/short) axes of symmetry of the exit shape.

Figure 2 shows schematically the arrangement of the PIV system, which was also reported in Refs. [8], [36], and [37]. This rig is positioned vertically under a 1.5 m  $\times$  1.5 m extraction hood located 2 m above the ground and 800 mm above the nozzle exit. A compressor supplied conditioned air to the test rig. The flow rate of the tube was metered by a pressure gauge and a Fisher & Porter tri-flat flow meter with an experimental accuracy of approximately 5%. All the five jets were measured at the same nominal Reynolds number of  $Re = 5 \times 10^4$ , where  $Re \equiv U_e D_e / \nu$ , with  $U_e$  being the exit bulk velocity ( $\approx 90$  m/s) and  $\nu$  the kinematic viscosity of fluid.

The air jet flows were seeded with small olive oil droplets, with an average diameter of about 1  $\mu\text{m}$ , generated by a Laskin nozzle particle generator. The droplets from the generator were divided into two streams, one was used to seed the jet flow and the other was for seeding the ambient air, as a 'co-flow', through a plastic tube coiled around the supply pipe with fine holes directed upwards at very low ejecting speed ( $< 1\%$   $U_e$ ). The momentum of the 'co-flow' was carefully maintained to be negligibly small so that it would not affect the jet.

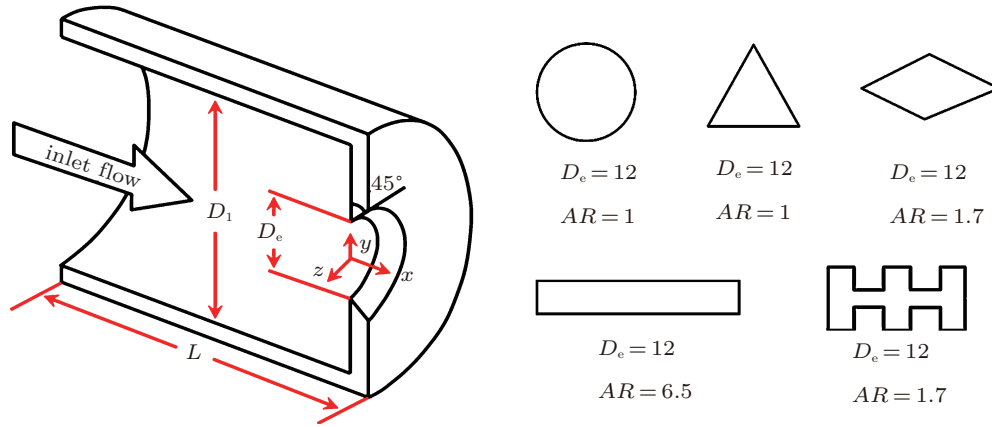


Fig. 1. (color online) Supply tube and orifice shapes with their equivalent diameter  $D_e$  (mm) and aspect ratio  $AR$ .

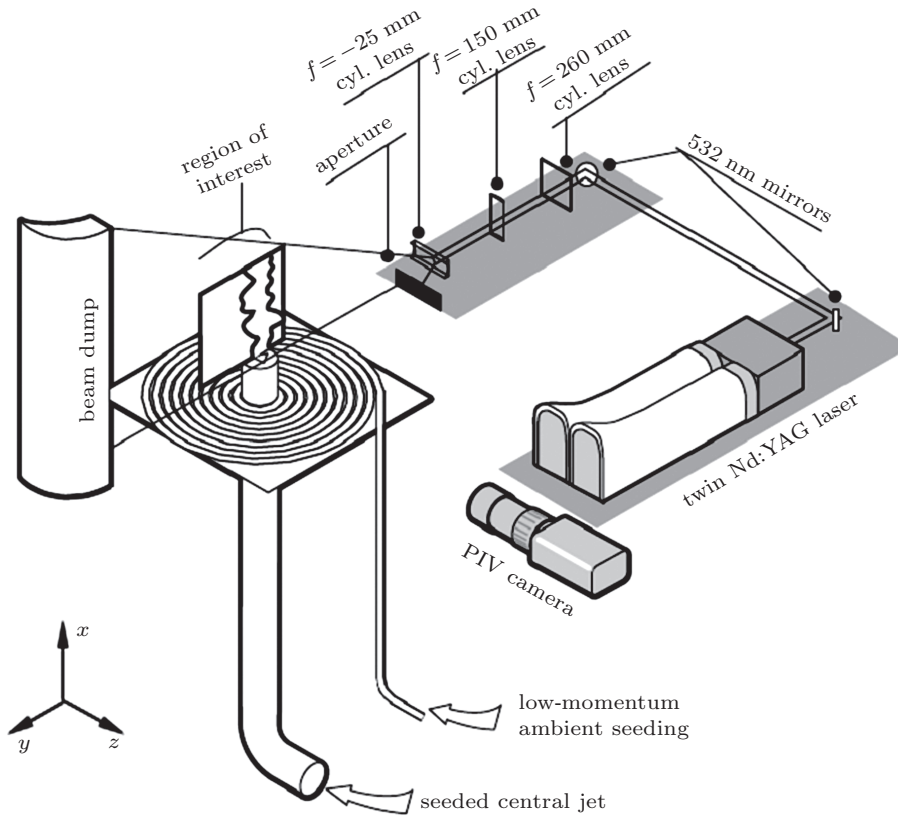


Fig. 2. Experimental arrangements of the PIV system and the coordinate system.

The velocity measurements were performed using particle image velocimetry, PIV, realized by a Quantel Brilliant Twins double-head Nd:YAG laser at a frequency of 10 Hz and power of 250 mJ per pulse at  $\lambda = 532$  nm. This laser was specially designed for PIV applications, each of the laser heads being independently triggerable. The temporal separation between laser pulses was adjusted from 10  $\mu$ s to 40  $\mu$ s, depending on the flow-field. The camera was a MegaPlus ES1.0, operated in triggered double exposure mode, with a  $1008 \times 1018$  pixel array. The collection optics comprised a Nikon ED 70 mm–300 mm (set to 110 mm) telephoto lens coupled to the camera C-mount with an adapter. The aperture was fully opened ( $f^\# = 4$ ). The imaging region was 100 mm by 100 mm,

so that each pixel images approximately 10  $\mu$ m in each direction. The thickness of the light sheet was about 1 mm. To measure a greater flow region, the nozzle was vertically translated once relative to the camera and laser sheet. This enabled the present measurements to cover the axial region  $0 < x < 17D_e$ , where  $x$  is the distance downstream from the orifice plate (upstream side, see Fig. 1). Data were collected from the camera at 20 Hz into a memory buffer on the data storage computer. All statistical fields of velocity were obtained from an ensemble of 500 instantaneous vector fields for each condition. Independence of all derived statistics from the ensemble size was confirmed by ensemble downsampling as reported by Mi *et al.*<sup>[37]</sup>

### 3. Results and discussion

#### 3.1. Mean velocity field

Figure 3 shows the normalized mean velocity ( $U/U_m$ ) contours in the  $xy$  and  $xz$  planes of the triangular, diamond, rectangular, notched-rectangular jet, as well as the central plane of the circular jet. The  $xy$  and  $xz$  planes are corresponding to the minor- and major-axis planes of noncircular jets respectively. Following most previous publications on the subject,  $U_m$  is chosen and denotes the maximum value of cen-

terline mean velocity  $U_c$ . For the present nozzles,  $U_m$  occurs at  $x/D_e \approx 0.5$  downstream from the exit plane because of the vena contracta. These measurement regions are located in the near-field over the range  $x/D_e \leq 8.2$ . Also shown are the streamlines in each plane. Obviously, the significant differences in the mean flow field among the five jets are revealed in Figs. 3(a)–3(e). It is worth noting that the mean velocity in the  $xy$  plane of the rectangular jet for  $x/D_e < 2$  is lower than that in the  $xz$  plane (Fig. 3(d)).

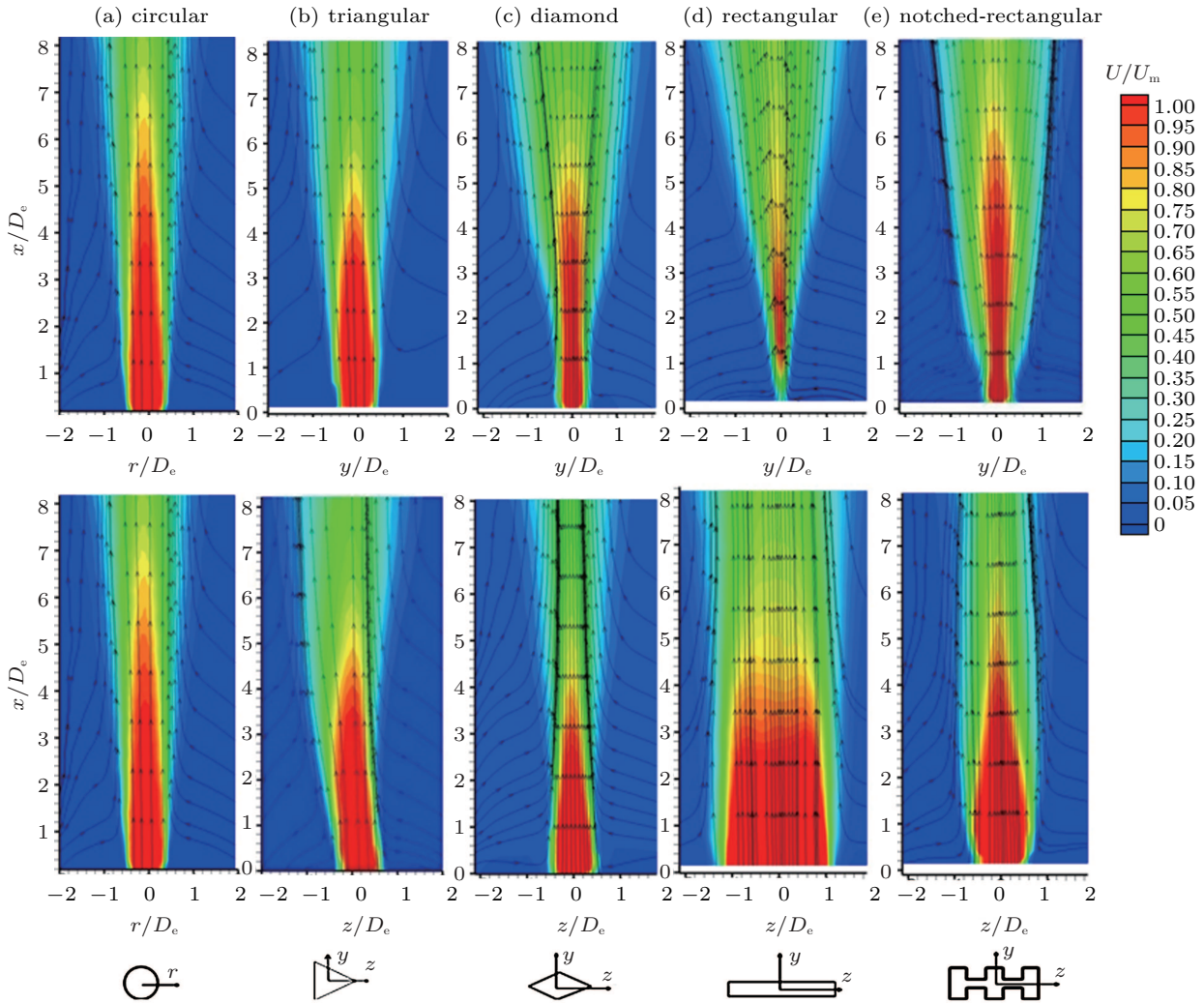


**Fig. 3.** (color online) Contours of normalized axial velocity in  $xy$  plane (up) and  $xz$  plane (down): (a) circular jet, (b) triangular jet, (c) diamond jet, (d) rectangular jet, (e) notched-rectangular jet at  $0 < x/D_e < 8.2$ . The streamlines in each plane are also displayed.

This is because that the width of the rectangular orifice is quite small, which means that the PIV resolution is not high enough for the velocity measurement in the  $xy$  plane of the rectangular jet for  $x/D_e < 2$ . Despite this, the centreline mean velocity and turbulent intensity of the rectangular jet can be obtained in the  $xz$  plane, where the velocity field is measured quite well. For the circular jet (Fig. 3(a)), it spreads out consistently as it proceeds downstream, and its central unmixed core, which is illustrated by the contours for  $U/U_m > 0.9$  is longer

than any other noncircular jet. In the  $xz$  plane of the triangular jet, the unmixed core bends towards the flat side ( $x/D_e < 0$ ) from the corner side ( $x/D_e > 0$ ), then returns back to the centreline. The force causing such a phenomenon is the lower pressure resulting from the larger scale vortical structures in the flat side ( $x/D_e < 0$ ).<sup>[7]</sup> For the diamond, rectangular, and notched rectangular jets, the  $xy$  and  $xz$  planes are corresponding to the minor- and major-axis planes respectively. In the  $xz$  plane, the three jets spread out rapidly from the exit plane to

$x/D_e \approx 2$ , then contracts slowly over the region of  $x/D_e = 3-7$ , and spreads continuously farther downstream. In the  $xy$  plane, the jets spread out very rapidly for  $x/D_e < 2$ , and the spreading rate becomes nearly constant for  $x/D_e > 2$ . It is also interesting to note that the length of the unmixed core of the rectangular jet seems to be the shortest among the five jets (Fig. 3(d)). This implies a highest rate of entrainment of the surrounding fluid for the rectangular jet.

To quantitatively compare the mean velocities of the five jets, figure 4 presents the streamwise variation normalized centreline velocity ( $U_m/U_c$ ), where  $U_m$  is the maximum centreline mean velocity. These data are extracted from the averaged PIV measurements over the range  $x/D_e < 17$ . Several observations can be made from Fig. 4. In the very near field, it is found that the length of the unmixed core  $L_c$  is shorter in noncircular jets ( $L_c = 0.7D_e \sim 3.6D_e$ ) than in the circular jet whose  $L_c = 4.0D_e$ , consistent with the above observation in mean velocity contours. Note that  $L_c$  is the length from the exit plane to the location where the centreline velocity is 98% of the maximum  $U_m$ . Particularly, among the present five jets, the rectangular has the shortest  $L_c (= 0.7D_e)$ , which is also shorter than that ( $L_c = 1.0D_e$ ) in the isosceles triangular jet studied in Mi *et al.*,<sup>[9,35]</sup> and that ( $L_c = 3.0D_e$ ) in the regular triangular jet investigated in Kanamori *et al.*<sup>[34]</sup>

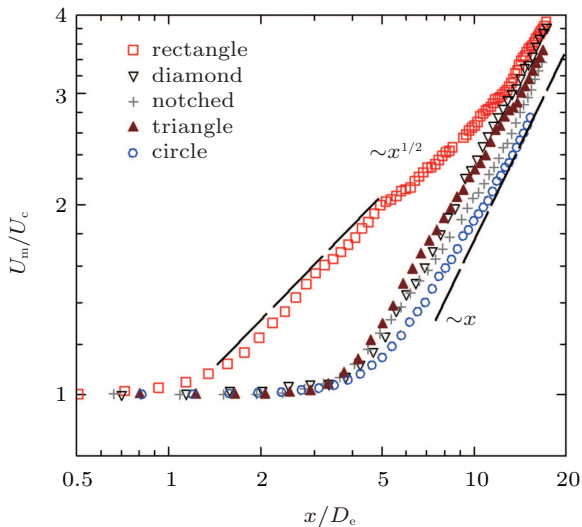


Fig. 4. (color online) Centerline evolutions of the normalized mean velocity in five jet flows in log-log plot.

Further downstream from the unmixed core ( $L_c < x/D_e < 10$ ),  $U_c$  for the noncircular jets decays faster than for the circular case. It is interesting to note that the rectangular jet decays most quickly, and  $U_m/U_c$  appears to asymptotically approach to the  $x^{1/2}$  dependence in a range of  $1.5 < x/D_e < 5$ , i.e.,  $U_m/U_c \sim x^{1/2}$ . Such a relationship is usually obtained in the far field of a plane jet,<sup>[38,39]</sup> which can also be treated as a rectangular jet with large aspect ratio ( $> 15 \sim 20$ ). In the present study, the aspect ratio of the rectangular jet is 6.5, ambient fluids are mainly entrained from long side (the  $y$  direction), only little surrounding fluids are entrained from short

side ( $z$  direction) (see Fig. 3(d)). Thus in the very near field ( $x/D_e < 5$ ), the rectangular jet flow acts like a plane jet. However, as the jet develops downstream, the initial shear layer becomes quite unstable, and any subtle perturbation can be amplified in this flow region. Vortex cores in the shear layer can form, evolve, and pair-up to form large eddies because of the large velocity gradient in the lateral and longitudinal directions. These large-scale eddies entrain more and more ambient fluids and break down and form smaller and smaller eddies.<sup>[1]</sup> Note that, more ambient fluids are entrained into the main jet from the long side ( $y$  direction) than from the short side ( $z$  direction), as vortex structures are much larger in the  $y$  direction than in the  $z$  direction. Thus the cross section of the rectangular jet gradually evolves into a round one. Therefore  $U_m/U_c$  is no longer following  $x^{1/2}$ , but gradually inclines to the  $x$  dependence, which is a typical characteristic of a round jet<sup>[1]</sup> (Fig. 4). The normalized centreline mean velocities of the other three noncircular jets also follow  $x$  dependence for  $x/D_e > 10$  (Fig. 4). This means that all the noncircular jets can evolve into round cross sections at a certain distance downstream. Bejan *et al.*<sup>[11]</sup> found that the principle for such a phenomenon is that the prevailing flow architecture provides greater access to the flow of momentum from the jet to the still surroundings.

For  $x/D_e > 10$ ,  $U_c$  data of all the jets over this measured range of  $x$  appear to follow the self-preservation relationship of a circular jet, i.e.,

$$\frac{U_m}{U_c} = K_u \left( \frac{x - x_0}{D_e} \right), \quad (1)$$

where  $K_u$  and  $x_0$  are respectively the mean-velocity decay parameter and virtual origin location and their magnitudes depend on the jet exit conditions.<sup>[40,41]</sup> Despite the fact that equation (1) may not be well reached in the present measurement range of  $x/D_e < 17$ , especially for the rectangular jet, the present data of  $K_u$  and  $x_0/D_e$  can also be estimated and shown in Table 1. Also, several previous data reported in the literature are given. Particularly, the definition and discussion of the axis-switching position  $L_{as}/D_e$  are presented later.

From Table 1, it is interesting to note that the values of slope  $K_u$  of all the noncircular jets are higher than those of the circular jets, which is consistent with the observation that the noncircular jets have a higher rate of entrainment of the surrounding fluid. In addition, for most of the noncircular jets whose  $AR$  values are  $1 \sim 2$ , their slope  $K_u$  values are close to 0.2, no matter how different are the experimental conditions (e.g., Reynolds number) and measurement techniques (e.g., PIV, HWA) used by different investigators. However, it should be noted that although the Reynolds numbers and measurement techniques are similar, the slope  $K_u$  values of the triangular jet in the present study and Hashiehba and Romano's study<sup>[6]</sup> are 0.18 and 0.24 respectively. Such a large difference may be caused by the small measurement ranges where the triangular jets cannot well reach self-similarity. This indicates

that the difference in total entrainment is more influenced by nearfield difference in entrainment than by far-field difference. For the noncircular jets with higher AR values their slope  $K_u$  values are far away from 0.2 (e.g.,  $K_u = 0.172$  for the present

rectangular jet with  $AR = 6.5$ ;  $K_u = 0.26$  for Hashiehbaf and Romano's<sup>[6]</sup> rectangular jet with  $AR = 3$ ). This supports that the large aspect ratio enhances mixing in the near filed,<sup>[19–21]</sup> no matter what the shape of the nozzle.

**Table 1.** Mean streamwise velocity decay parameters on the jet centreline and axis-switching position  $L_{as}/D_e$  for various jets.

1st investigator (year)	Nozzle shape	AR	Measurement techniques	$K_u$	$x_0/D_e$	Range of $x/D_e$	$Re \approx$	Axis-switching position $L_{as}/D_e$
Present	circle	1	PIV	0.160	-1.58	10~17	$5 \times 10^4$	-
	triangle	1		0.180	-2.5			1.7
	diamond	1.7		0.204	-1.44			2.5
	rectangle	6.5		0.172	-5.26			10
	notched-rect	1		0.201	0.17			3.0
Hashiehbaf (2013)	triangle	1	PIV	0.24	-0.65	6~20	$3.5 \times 10^4$	1.5
	rectangle	3		0.26	1.03			2.5
	square	1		0.18	-1.76			1.0
Mi (2010)	square	1.0	HWA	0.203	0.5	8~40	$1.5 \times 10^4$	-
	rectangle	2.0		0.200	-0.9	8~40		-
	triangle	1.0		0.203	-1.0	5~40		-
	isosceles-tri	2.5		0.200	-3.6	5~40		-
Quinn (2005)	triangle	1.0	HWA	0.196	-0.39	20~52	$1.84 \times 10^5$	1.3
	isosceles-tri	1.72		0.207	-0.18			2.0
Kanamori (2011)	triangle	1	HWA	-	-	-	$5 \times 10^4$	0.85
	square	1	HWA	-	-	-		0.52
	pentagon	1	HWA	-	-	-		0.38
	hexagon	1	HWA	-	-	-		0.32

Besides the centerline velocity, the half-width at which the mean velocity is half of the centerline velocity is usually used to reveal the mixing characteristics of jet flows. Figure 5 shows the half-widths in the  $xy$  and  $xz$  planes, and half-width equivalent radius defined as  $B = (y_{1/2}z_{1/2})^{1/2}$ . Obviously, the spreading rates of the noncircular jets based on the half-widths are greater than those of the circular jets at  $x/D_e > 5$  (Figs. 5(a) and 5(b)). This is consistent with the higher rate of decay for the noncircular jet. Compared with that of the noncircular jet, the half-width equivalent radius of the rectangular jet is high (Fig. 5(b)). This suggests that the rectangular jet with high aspect ratio interacts with surrounding fluids greatly so that the jet spreads out fast and enhances mixing.

In particular, from Fig. 5(a), it is found that there is a position ( $L_{as}$ ) at which two half-widths in different planes equal each other, i.e.,  $y_{1/2}(L_{as}) = z_{1/2}(L_{as})$ , for each of the diamond, rectangular, notched-rectangular jet flows. For the triangular jet, the position is where  $z_{1/2}^+(L_{as}) = z_{1/2}(L_{as})$ . The results of  $L_{as}$  for the present noncircular jets are shown in Table 1, which also includes previous data reported in the literature. Such a phenomenon is called “axis-switching” which is considered to be one of key factors for noncircular jets to have more effective mixing performance than for comparable circular jets.<sup>[8,14,17,21,42–44]</sup> This phenomenon has also been observed in the comparable noncircular jets experimentally.<sup>[14,34,43]</sup> In the present study, the “axis-switching” position for the

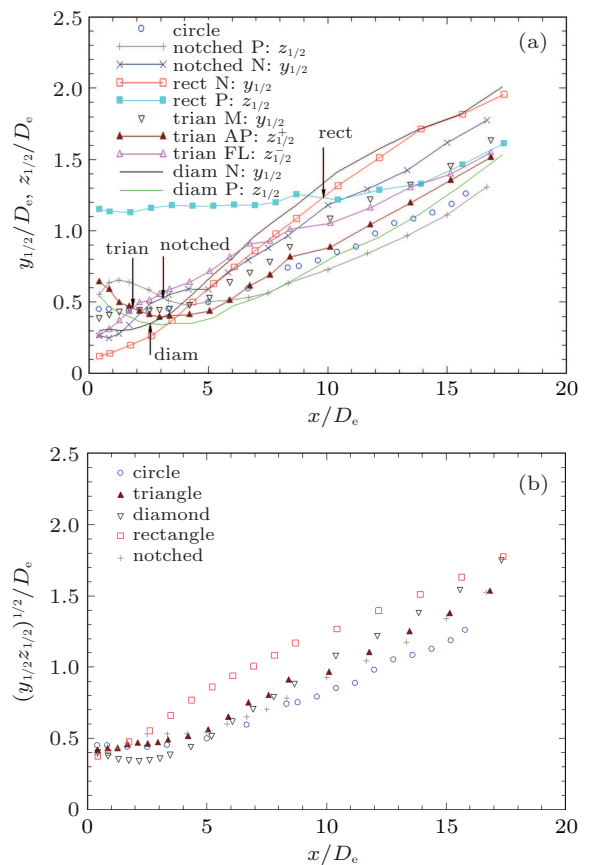


**Fig. 5.** (a) The half-widths in the  $xy$  and  $xz$  planes, and (b) the half-width equivalent radii of the circular and noncircular jets. Note that the arrows point to the positions where the “axis-switching” phenomena happen for different noncircular jets.

rectangular jet is furthest ( $L_{as} = 10D_e$ ), while the triangular jet has the nearest “axis-switching” position ( $L_{as} = 1.7D_e$ ) (see Table 1). For the diamond and notched-rectangular jets,  $L_{as} = 2.5D_e$  and  $3.0D_e$  respectively. This suggests that non-circular jet with high aspect ratio can postpone the “axis-switching” phenomenon (see Fig. 5(a)). Kanamori *et al.*<sup>[34]</sup> found that the location of one complete cycle of axis-switching shifted downstream of the jet with reducing the number of polygon sides, i.e.,  $L_{as} = 0.85D_e$  for the regular triangular jet, while  $L_{as} = 0.32D_e$  for the hexagon jet (Table 1). Thus, it can induce that the location of the ‘axis-switching’ phenomenon shifts upstream as the orifice shape gradually evolves into circular shape. This is consistent with the previous findings<sup>[4]</sup> that axis switching strongly depends on jet initial condition.

### 3.2. Fluctuating velocity field

To better understand the mixing characteristics of noncircular jets, the contours of normalized streamwise root mean square (RMS) ( $u'/U_m$ ) in the five jets are shown in Fig. 6. Here,  $u'$  is the RMS fluctuating velocity, defined as  $u' =$

$\langle u^2 \rangle^{1/2}$ . As seen for all configurations, the high value (the contours for  $U/U_m > 0.9$ ) of  $u'/U_m$  happens in the shear layers of the jet flows at  $x/D_e < 3 \sim 4$ . Note that the high fluctuating velocity (the contours for  $U/U_m > 0.9$ ) in Fig. 6(d) in the  $xy$  plane of the rectangular jet for  $x/D_e < 2$  is caused by the ineffective resolution for velocity measurements in the region, which is also observed in the mean velocity field (Fig. 3(d)). It seems that the rectangular jet has the largest region of high values of  $u'/U_m$  in the  $xz$  plane in the five jets (Fig. 6(d)), while the notched-rectangular jet has the smallest region (Fig. 6(e)). As is well known, very large vortex structures can roll-up in the shear layer at each long side of the rectangular jet, then they interact with each other and with ambient fluids, resulting in the strongest fluctuating velocity field. For the notched-rectangular jet, the vortex structures are very intense, three-dimensional and complex and small in size. It is also interesting to note that the high value region in the diamond jet is larger than in the triangular jet (Figs. 6(b) and 6(c)). This may indicate that the corner part has a stronger ability to enhance mixing than the flat part.

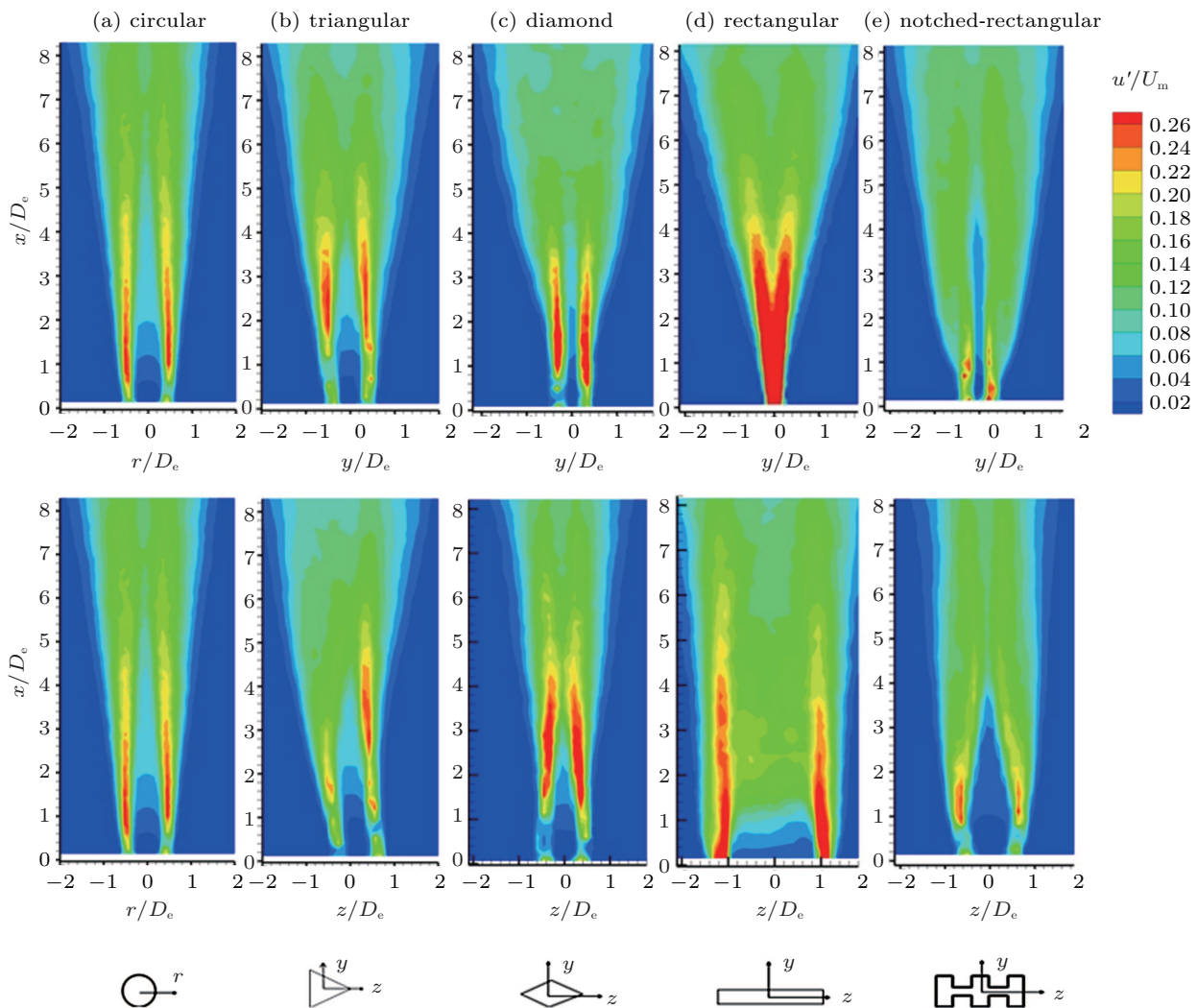


Fig. 6. (color online) Contours of normalized streamwise RMS ( $u'/U_m$ ) in  $xy$  and  $xz$  planes for (a) circular jet, (b) triangular jet, (c) diamond jet, (d) rectangular jet, and (e) notched-rectangular jet in a range of  $0 < x/D_e < 8.2$ .



To quantitatively compare the evolution of the turbulent field, figure 7 presents the variations of normalized stream-wise turbulent intensity  $u'/U_c$  with  $x/D_e$ . For comparison, the results of the circular and triangular jets cited from Refs. [9] and [33] are also added there. Obviously, the value of  $u'/U_c$  in the rectangular jet increases fastest with  $x$  increasing in all the jets. When the jet develops downstream, there are clear humps on the curves of  $u'/U_c$  versus  $x/D_e$  for the rectangular and triangular jets, while no humps occur on the curves for the circular, diamond, notched-rectangular jets. This is consistent with Mi and Nathan's<sup>[9]</sup> observations of nine turbulent jets, among which, the isosceles triangular jet has the most significant hump. The reason for such humps occurring in rectangular jet and triangular jet is that vortex structures generated from the flat side or long side are large and regular, and then they are broken up at the end of the unmixed core, which can cause an intense fluctuating velocity. For the diamond and notched-rectangular jets, the vortex structures are small and three-dimensional, thus cannot form the hump, even if they are also broken up at the end of the unmixed core.

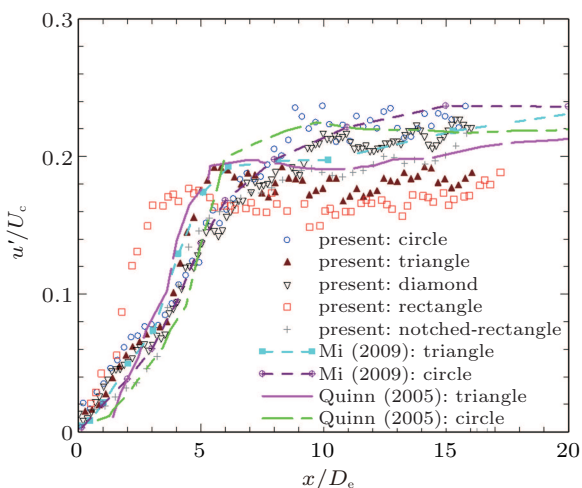


Fig. 7. (color online) Centerline evolutions of turbulent intensity  $u'_c/U_c$  in the five jets.

For the further downstream part, the turbulent intensities of the five jets appear to converge to their asymptotic values. Actually, the RMS velocity profiles of the present noncircular jets are far from the converged ones in the measurement range, with the profiles in the  $xy$  plane and  $xz$  plane retaining significant differences at  $x/D_e = 15$  (not shown here). It is interesting to note that the turbulent intensity of the noncircular jet at  $x/D_e > 10$  is lower than that of the circular jet, and the rectangular jet has the lowest turbulent intensity. Such a trend is correlated with the hump in the jet flow, which suggests that the more obvious the hump, the lower the turbulent intensity will be. However, it is worth noting that the turbulent intensity of the noncircular jet is higher than that of the circular jet in the self-preservation field ( $x/D_e > 30$ ).<sup>[9,33]</sup>

## 4. Conclusions

In the present study, we investigate turbulent free jets issuing, respectively, from circular, triangular, diamond, rectangular, and notched-rectangular orifice plates in the near and transition regions at  $Re = 5 \times 10^4$  using the planar PIV technique. Detailed comparisons of mean and turbulence fields among the five jets within  $17D_e$  are made. From the results reported in the present paper, several main conclusions can be drawn below.

(i) Compared with the circular jet, the noncircular jet can enhance entrainment rate, which is indicated by the higher rate of mean velocity decay and spread, shorten the length of the unmixed core, and expedite the increase of turbulent intensity. The present rectangular jet ( $AR = 6.5$ ) produces the greatest decay rate of the near-field mean velocity in all the jets of the present study.

(ii) The “axis-switching” phenomenon is observed in all the present noncircular jets and greatly influenced by the nozzle shape. The noncircular jet with high aspect ratio can postpone the position at which the ‘axis-switching’ phenomenon occurs. The present rectangular jet has the furthest axis-switching position. This supports the fact that axis switching phenomenon strongly depends on jet initial condition

(iii) There are humps on the curves of the centerline variation of the turbulence intensity with  $x/D_e$  for the rectangular and triangular jets, but not for the circular jet nor for diamond jet nor for notched-rectangular jet. The most obvious hump is observed in the rectangular jet in which large and regular vortex structures can be generated from the exit plane and broken up at the end of the unmixed core, hence resulting in high turbulent intensity.

## References

- [1] Ball C, Fellouah H and Pollard A 2012 *Prog. Aerospace Sci.* **50** 1
- [2] Luo Z B L and Xia Z X 2008 *Chin. Phys. Lett.* **25** 612
- [3] Mi J C and Feng B P 2011 *Chin. Phys. B* **20** 074701
- [4] Gutmark E and Grinstein F 1999 *Ann. Rev. Fluid Mech.* **31** 239
- [5] Quinn W, Azad M and Groulx D 2012 *AIAA Journal* **51** 70
- [6] Hashiehbab A and Romano G P 2013 *Int. J. Heat Fluid Flow* **44** 208
- [7] Xu M Y, Zhang J P, Mi J C, Nathan G J and Kalt P A M 2013 *Sci. China Ser. G* **56** 1176
- [8] Xu M Y, Zhang J P, Mi J C, Nathan G J and Kalt P A M 2013 *Chin. Phys. B* **22** 034701
- [9] Mi J and Nathan G J 2010 *Flow Turbul. Combust.* **84** 583
- [10] Mi J C and Du C 2011 *Chin. Phys. B* **20** 124701
- [11] Bejan A, Ziaei S and Lorente S 2014 *Sci. Rep.* **4** 04730
- [12] Miller R, Madnia C and Givi P 1995 *Comput. Fluids* **24** 1
- [13] Grinstein F 2001 *J. Fluid Mech.* **437** 69
- [14] Koshigoe S, Gutmark E, Schadow K and Tubis A 1989 *AIAA Journal* **27** 411
- [15] Zhang J P, Xu M Y and Mi J C 2014 *Chin. Phys. B* **23** 044704
- [16] Zaman K B M Q 1996 *J. Fluid Mech.* **36** 1
- [17] Gutmark E, Schadow K, Parr T, Hanson-Parr D and Wilson K 1989 *Expt. Fluids* **7** 248
- [18] Cabaleiro J M and Aider J-L 2014 *Phys. Fluids* **26** 031702
- [19] Deo R C, Mi J and Nathan G J 2007 *Exp. Therm. Fluid Sci.* **31** 825
- [20] Quinn W 1992 *Exp. Therm. Fluid Sci.* **5** 203

- [21] Hussain F and Husain H 1989 *J. Fluid Mech.* **208** 257
- [22] Xu G and Antonia R A 2002 *Expt. Fluids* **33** 677
- [23] Mi J, Nobes D S and Nathan G J 2001 *J. Fluid Mech.* **432** 91
- [24] Deo R C, Mi J and Nathan G J 2008 *Phys. Fluids* **20** 075108
- [25] Dimotakis P E 2005 *Ann. Rev. Fluid Mech.* **37** 329
- [26] Xu M, Pollard A, Mi J, Secretain F and Sadeghi H 2013 *Phys. Fluids* **25** 035102
- [27] Mi J, Xu M and Zhou T 2013 *Phys. Fluids* **25** 075101
- [28] Dowling D R and Dimotakis P E 1990 *J. Fluid Mech.* **218** 109
- [29] Azad M, Quinn W and Groulx D 2012 *Exp. Therm. Fluid Sci.* **39** 237
- [30] Quinn W R 2007 *Eur. J. Mech. B: Fluids* **26** 583
- [31] Quinn W R 1994 *AIAA Journal* **32** 547
- [32] Quinn W and Militzer J 1988 *Phys. Fluids* **31** 1017
- [33] Quinn W 2005 *Expt. Fluids* **39** 111
- [34] Kanamori A, Hiwada M, Oyakawa K and Senaha I 2011 *Open Transport Phenomena J.* **3** 9
- [35] Mi J, Nathan G J and Luxton R E 2000 *Expt. Fluids* **28** 93
- [36] Mi J, Kalt P and Nathan G 2010 *Flow Turbul. Combust.* **84** 565
- [37] Mi J, Kalt P, Nathan G J and Wong C Y 2007 *Expt. Fluids* **42** 625
- [38] Deo R C, Nathan G J and Mi J 2013 *Phys. Fluids* **25** 015115
- [39] Landel J R, Caulfield C and Woods A W 2012 *J. Fluid Mech.* **692** 347
- [40] Lipari G and Stansby P K 2011 *Flow Turbul. Combust.* **87** 79
- [41] Uddin M and Pollard A 2007 *Phys. Fluids* **19**
- [42] Schadow K, Gutmark E, Parr D and Wilson K 1988 *Expt. Fluids* **6** 129
- [43] Ho C and Gutmark E 1987 *J. Fluid Mech.* **179** 383
- [44] Husain H and Hussain A 1983 *Phys. Fluids* **26** 2763